JOURNAL OF CATALYSIS **160,** 279–289 (1996)
ARTICLE NO. 0146

Characterization and Catalytic Properties of Sulfated ZrO_2–TiO_2 Mixed Oxides

Ferenc Lónyi, József Valyon,[1] József Engelhardt, and Fujio Mizukami[2]

Central Research Institute for Chemistry of the Hungarian Academy of Sciences, H-1525 Budapest, P.O. Box 17, Hungary

Received August 31, 1995; revised January 5, 1996; accepted January 10, 1996

The acidity of sulfated zirconia–titania preparations was studied using NH_3, pyridine, and benzene as the probe molecule. Temperature-programmed desorption curves of ammonia and the IR spectra of adsorbed pyridine were determined to distinguish acid sites. The Brønsted acidic strength of the surface hydroxyl groups was correlated with the red shift of the ν_{OH} IR band induced by adsorption of benzene. The conversion of *n*-hexane was used as the catalytic test. The thermally effected textural and structural changes were followed by thermogravimetry, X-ray diffraction, energy-dispersive X-ray analysis, and surface area measurements. Sulfate and titania were found to hinder the aggregation of the metal oxide component. The weight-specific concentration of strong Lewis and Brønsted acidic sites were found higher in the zirconia-rich mixed oxides than in SO_4^{-2}/ZrO_2, but, no new kind of acidic center was detected. The strongest acidic sites are Lewis centers. The sulfate treatment of the oxides resulted in the formation of new, strong Brønsted sites. Regardless, whether the basic probe was protonated (as pyridine) or not (as benzene) the negative charge on the conjugated base of the Brønsted acid increased upon adsorption. This is indicated by the induced red shift of the $\nu_{S=O}$ band of the surface sulfate group. This effect decreases the acid strength of the proton to an extent depending on the degree of electron donation and the volume available for delocalization of the electrons. The use of basic probes is not suggested for comparing the acid strength of catalysts much different in structure and composition.

INTRODUCTION

Superacids, defined as materials with an acid strength stronger than 100% sulfuric acid, can activate paraffins and effect their catalytic transformation into fine chemicals or higher octane-grade branched isomers at lower reaction temperatures than conventional acid catalysts. The lower reaction temperature represents energy saving and favors the formation of the desired branched products (1). The use of liquid phase superacid catalysts presents serious problems: It is difficult to separate the acid and the product stream, large amount of catalyst is usually required, and the catalyst waste is significant, causing an environmental hazard. Furthermore, the cost of process installation and maintenance is high since the liquid acids are very corrosive. It has been sought for long to replace liquid acid for solid showing comparable catalytic properties (2). Strongly acidic sites can be created within the pores of some high-silica zeolites, but, over zeolite catalysts the conversion of paraffins into branched products is low due to steric constraints.

In relation to above problems the discovery of strong nonzeolitic solid acids was a breakthrough. Metal oxides, especially ZrO_2, TiO_2, Fe_2O_3, and zirconia-containing mixed oxides modified by sulfate ions have been found to be promising catalysts for low-temperature esterification, isomerization, alkylation, and cracking (3, 4). Due to their high thermal stability and low reducibility much attention has been focused on the sulfate promoted zirconium oxides (3–11). Sulfate is usually introduced by immersing zirconium hydroxide in a dilute solution of sulfuric acid or by impregnation from a solution of ammonium sulfate. The properties of the catalyst are strongly influenced by the preparation conditions, including the precipitation conditions of the hydroxide gel, and the thermal treatments of the gel prior to and after introduction of sulfate (4–9).

The structure of the surface sulfate species and the way that the catalytically active acidic centers are generated are not fully understood yet. No agreement has been reached about the strength and the nature of the acidic sites. It was found that the sulfur containing species are bound to the oxide through two or more S–O–Zr bridges and carry double or single S=O oscillators, respectively (12–16). The different sulfate species were suggested to develop at different kinds of surface locations; an abundant on the less energetic flat crystal faces of ZrO_2, and another on the defective sites (6, 17). The presence of polynuclear complex sulfates (possibly of the $[S_2O_7]^{2-}$ type) at higher sulfate loading was also substantiated (18). It was shown by Ward and Ko (12) that the chemical state of sulfate groups depends on the conditions of catalyst pretreatment. After activation at low

[1] To whom correspondence should be addressed. Fax: (36-1) 212-5020. E-mail: h6133lon@ella.hu.

[2] Current address: National Institute of Materials and Chemical Research, 1-1 Higashi, Tsukuba, Ibaraki 305, Japan.

0021-9517/96 $18.00

temperatures it has partially ionic character with the S=O bond order less than two, whereas upon treatment at higher temperatures the sulfate is converted into a strongly covalent species with the S=O bond order close to two. These latter species were suggested to be responsible for generating the strongly acidic active centers.

The importance of Brønsted acidic sites in the development of the catalytic activity of the sulfate-doped zirconia have been demonstrated by several authors (e.g., 6–9, 12). It is thought that Brønsted acidity is predominantly determined by the sulfate loading, although other factors can also have significance. Sulfate species are Lewis acids or by attracting electrons they generate Lewis acid sites on the surface of zirconia. The Lewis acid centers increase the Brønsted acidic strength of surface hydroxyl groups. These ideas are very similar to that suggested for acidic zeolites (19).

The highly acidic, presumably superacidic nature of sulfated zirconia has been shown by IR and H^1 MAS NMR spectroscopic measurements (20–22). Two types of isolated surface OH groups were shown on nonsulfated zirconia (22). IR bands were assigned to terminal and bridging hydroxyls. Modification with sulfuric acid eliminated the terminal OH groups, while the acid strength of the bridging hydroxyls increased. In addition, new Brønsted acid sites were generated as indicated by the appearance of a new, very broad band in the OH region. Based on H^1 MAS NMR data it was concluded that more acidic protons are present in sulfated zirconia than in H-ZSM-5. It was suggested that the acidic OH group is linked to sulfur and the proton is bridging to a neighboring oxide ion of the ZrO_2 support. These findings are in accordance with the catalytic activity of the preparations in acid-catalyzed reactions, such as oligomerization of olefines or isomerization of alkanes. However, when a weak base probe molecule, for instance CCl_3CN or CD_3CN, was used and the acidity was correlated with the difference of the chemical shifts before and after adsorbing the probe the H^1 MAS NMR data suggested that the sulfated zirconia contains the weakest Brønsted acidic centers among the catalysts studied, even weaker centers than nonsulfated zirconia. As an attempt to resolve the controversy between the weak acidity and the high catalytic activity it was assumed that the reaction rate is enhanced by the favorable stabilization of the reaction intermediates on the sulfated surface (21).

The catalytic activity of sulfated zirconia is rapidly lost due to sintering and coking. More active and stable catalyst can be obtained by introduction of transition metals, especially noble metals (21, 23, 24). The thermal resistance of zirconia against sintering can be considerably improved by incorporation of a second oxide (25, 26). It has been shown that the surface area of ZrO_2–TiO_2 mixed oxides changes parallel with the titania content until it passes through a maximum at about equimolar composition.

It is well known that mixing two oxides can create acidity. Tanabe's model (2) predicts Lewis acidity for zirconia-rich and Brønsted acidity for titania-rich chemically mixed TiO_2/ZrO_2. Tanabe's hypotheses was tested by studying the adsorption of pyridine. It was found that in TiO_2/ZrO_2 binary oxides the number of Lewis sites per square meter was about the same as that in the pure oxides (26b).

In a previous paper (27) we reported that in sulfated zirconia–titania mixed oxides the crystallization and the phase transformation of the zirconia, furthermore; the decomposition of sulfate takes place at higher temperature than in ZrO_2 or SO_4^{2-}/ZrO_2. The higher thermal resistance is advantageous since it allows the regeneration of deactivated catalysts by high-temperature calcination. However, the role of titania in the development of the acidic and catalytic properties of the preparations is not known yet. In the present paper the acidic and catalytic properties of sulfated ZrO_2–TiO_2 mixed oxides are discussed. In connection with this problem the probe-molecule method of acidity measurement is critically evaluated.

EXPERIMENTAL

Catalyst Preparation

Metal hydroxides were precipitated by dropping a solution of Zr-*n*-propoxide, or Zr-*n*-propoxide–Ti-*i*-propoxide mixture containing 0.16 mol metal into 70 ml of 1.5 *M* aqueous NH_3 solution under continuous stirring at 343 K. The temperature was raised to 363 K and the gel formed was stirred until almost all the liquid phase was removed by evaporation (2–3 h). The product was dried at 383 K overnight. The dried gel was contacted with 0.25 *M* H_2SO_4 solution (5 ml solution/1 g sample) under continuous stirring for 1 h and then filtered (not washed) and dried again at 383 K overnight. The sulfate-promoted zirconia catalysts were obtained by calcining the acid-treated hydroxide gel in air at 823, 923, or 973 K for 3 h.

The Zr-*n*-propoxide used was a 1-propanolic solution containing 21.6 wt% Zr (Aldrich, analytical grade). The Ti-*i*-propoxide was a product of Kanto Chemicals (Japan) and was of >97% purity.

Catalyst Characterization

Thermal studies. The thermoanalytical curves of the preparations were determined using a TG-DTA 2000 type thermal analyzer (MAC Science, Japan). Samples (15–35 mg) were heated up in air flow (~20 ml/min) at a rate of 5 K/min. α-Alumina (pretreated at 1373 K) was used as reference solid. Data were collected and analyzed by a computer connected to the system.

X-ray diffraction. The X-ray diffraction patterns of the samples were recorded by a MAC Science MXP18 diffractometer using Cu $K\alpha$ radiation ($\lambda = 1.5405$ nm).

Specific surface area. Adsorption isotherms of nitrogen were determined at 78 K. The surface area was calculated by the BET method.

Energy dispersive X-ray analysis (EDX). EDX measurements were carried out on a Hitachi S-800 electron microscope with a Kevex Delta system attached. The parameters were as follows: accelerating voltage, 15 kV; accumulation time, 100 s, window width, 8 μm. The surface molar composition was determined by the Asa method (Zaf-correction, Gaussian approximation).

Temperature-programmed desorption (TPD) of NH_3. A Shimadzu DT-40 thermal analyzer was used. A sample (300 mg) with a particle size of 0.5–1.0 mm was placed into the sample holder of the microbalance and heated up to 773 K in vacuum at a heating rate of 10 K/min. After 1 h treatment at 773 K, the sample was cooled to room temperature and purged with flowing ultrahigh purity (UHP) helium (100 ml/min) for 5 min. The gas flow was changed to a flow of 2% NH_3/He. In about 1 h, when no further weight change could be observed, the gas flow was stopped. In order to remove the weakly adsorbed NH_3, sample was evacuated at 423 K for 1 h. After an additional 1-h purging with He (100 ml/min) at 423 K sample was heated up at a rate of 10 K/min to 973 K. Using a new portion of the sample a blank experiment was carried out under identical conditions, but, without adsorbing NH_3. The NH_3 TPD curve was derived from the TG data corrected with the results of the blank. The accuracy of the measurement decreases as correction becomes more substantial, i.e., at temperatures above 823 K where the overwhelming part of the weight loss is due to decomposition of sulfate.

FTIR measurements. The infrared spectroscopic investigations were carried out using a Nicolet 5PC FTIR spectrometer equipped with TGS detector. Self-supporting pellet of 5–10 mg/cm^2 "thickness" was pressed from the sample, placed into an IR cell, heated up gradually in 100 K increments to 773 K in a flow of dry oxygen (500 ml/min), and activated for 1 h. The oxygen flow was stopped and the sample was evacuated (10^{-3} Torr) at 773 K for 1 h. Following a 5-min contact with pyridine at 2 Torr pyridine pressure at room temperature sample was evacuated subsequently at 423, 523, and 673 K for 1 h each time. After each evacuation a spectrum was recorded at room temperature at a nominal resolution of 4 cm^{-1}. Two hundred scans were averaged. Benzene adsorption measurements were carried out essentially the same way, but, no postadsorption evacuation was applied. The benzene pressure was 5 Torr, and the contact time was 5 min.

Catalytic conversion of n-hexane. An atmospheric flow-through microreactor was used at 423 K. A catalyst sample (200 mg) with a particle size of 0.25–0.5 mm was placed into a quartz U-tube reactor of 4-mm internal diameter and pretreated at 773 K in dry oxygen flow (20 ml/min) for 1 h. Flow was changed then to helium and the sample was cooled to 423 K. The reaction was started by switching to a 5 ml/min *n*-hexane/helium flow prepared by passing helium through a saturator containing *n*-hexane (>90% purity, Reanal, Hungary) at 273 K. The partial pressure of *n*-hexane was 46 Torr. The reactor outlet was analyzed first after 5 min reaction time using on-line GC with a Petrocol DH fused silica capillary column. The results were corrected for the impurities in the reactant.

RESULTS

Structural and Thermochemical Properties

DTG and DTA curves of sulfated ZrO_2 and ZrO_2–TiO_2 catalysts are shown in Figs. 1 and 2. The sulfate of the zirconia-rich preparations ($\geq$50 mol%ZrO_2) decomposes in two steps. A sharp and a broad peak appear on the DTG curve at about 953–963 K and 1053–1073 K, respectively (Fig. 1a). In contrast, the release of sulfate from the titania-rich sample generates a single broad peak with a maximum at about 973 K. It is evident that sulfate content of the samples, calculated from the weight loss above 873 K, must depend on the pretreatment conditions. Thus, less sulfate is held in the samples treated at 923 K than in those treated at 823 K (cf. Figs. 1a and 2a). Interestingly, the sulfate content of the zirconia-rich samples calcined at 823 K is essentially the same and about equal to the possible maximum calculated assuming that the total amount of sulfate present in the sulfuric acid solution used for preparing the catalyst was retained by the solid, i.e., 1.25 mmol SO_4^{2-}/g_{cat} or 12 wt%.

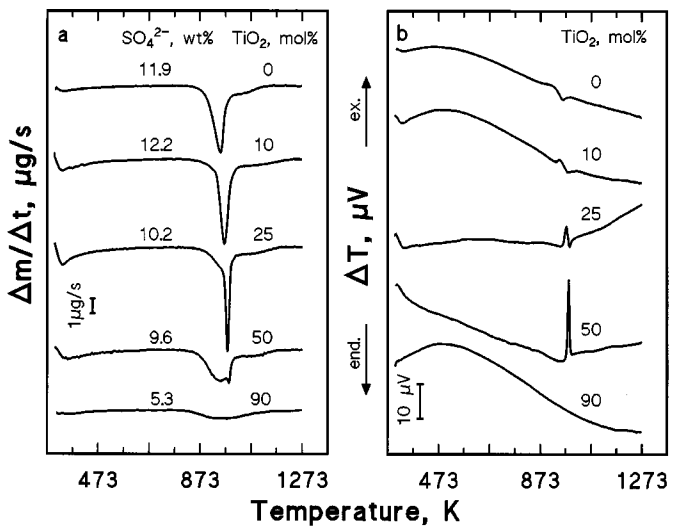

FIG. 1. DTG (a) and DTA (b) curves of sulfated ZrO_2 and ZrO_2–TiO_2 catalysts. Gels treated with sulfuric acid were precalcined in air at 823 K for 3 h. Air-dry samples were heated up at a rate of 5 K/min. The sulfate contents given in percentages were obtained as the weight loss above 823 K.

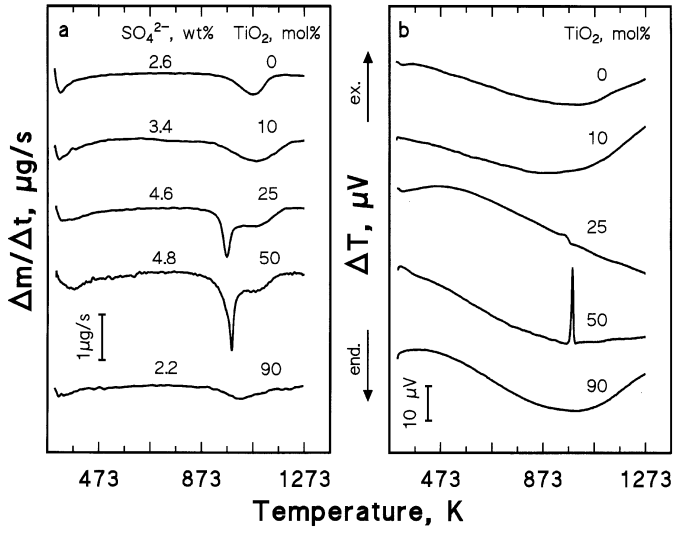

FIG. 2. DTG (a) and DTA (b) curves of sulfated ZrO_2 and ZrO_2–TiO_2 catalysts precalcined at 923 K. For details see legend to Fig. 1.

The XRD analysis indicated that sulfated samples treated at 823 K are amorphous except the one containing 90 mol% TiO_2 that is for the most part crystalline anataze. On 923 K the zirconia-rich samples become ordered mainly into tetragonal ZrO_2. The equimolar ZrO_2–TiO_2 preparation remains amorphous; its crystallization takes place at higher temperature resulting in the formation of $TiZrO_4$. The specific surface area of zirconia-rich, sulfated samples considerably increases with the TiO_2 content and also depends on the temperature of pretreatment (Table 1).

In contrast to sulfated ZrO_2, the nonsulfated ZrO_2 becomes crystalline upon treatment at 823 K. Beside some tetragonal phase the sample consists predominantly the monoclinic crystal form. No crystallization of the nonsulfated sample containing 50 mol% TiO_2 occurred up to 823 K; however, following treatment at 923 K crystalline $TiZrO_4$ phase was identified by XRD (Table 1).

It was shown earlier (27) that the addition of sulfate and titania as a second oxide to zirconia hinders the crystallization of the originally amorphous preparation. The change in the crystallization kinetics is reflected by the shift of the exothermal DTA peak to higher temperatures. The endothermal decomposition of sulfate and the exothermal crystallization of zirconia occurs in about the same temperature range. Data suggest that at low titania contents both processes are slow and the net thermal effect generates weak, ill-defined DTA peaks between 873 and 1073 K (Fig. 1b, curves for 0–25 mol% TiO_2–ZrO_2). At higher titania contents the samples of increased surface area go through fast phase transformation. The rapid evolution of the crystallization heat results in the appearance of the sharp DTA peak superimposed on the broad peak of the endothermic sulfate decomposition. Due to the heat effect, the corresponding DTG peak of sulfate decomposition takes on complex peak profile (Figs. 1a and 1b; 25–50 mol% TiO_2–ZrO_2). In accordance with the result of the X-ray analyses the appearance of the crystallization peak on the DTA curve of the equimolar zirconia–titania preparation clearly indicates that sample remained X-ray amorphous after the thermal treatment at 923 K (Fig. 2b).

The surface molar composition of the preparation containing equivalent amounts of ZrO_2 and TiO_2 was determined by EDX (Table 2). The surface of the dried gel was found to be richer in titania than the bulk. On calcination above 823 K a single phase of homogeneous composition develops in the nonsulfated sample while a significant

TABLE 1

Specific Surface Area[a] (m^2/g) and Crystallographic Properties of Sulfated ZrO_2 and ZrO_2–TiO_2, Catalysts Pretreated[b] at Different Temperatures

ZrO_2–TiO_2 composition (mol%)	Pretreatment temperature (K)		
	823	923	973
100–0	72.7, A(C[c, d])	90.2, C[e]	—
90–10	128.4, A	119.4, C[e]	—
75–25	192.2, A	112.7, C[e]	—, C[e]
50–50	257.9, A (A[c])	121.4, A (C[c, f])	63.7, C[f]
10–90	129.3, C[g]	—, C[g]	—

Note. A, amorphous; C, crystalline.

[a] Calculated from N_2 adsorption isotherm by the BET method.

[b] Metal hydroxide was precipitated, treated with sulfuric acid, and calcined in air at the given temperature for 3 h.

[c] Nonsulfated sample.

[d] Monoclinic and some tetragonal phase.

[e] Tetragonal zirconium dioxide.

[f] Crystalline $TiZrO_4$.

[g] Anatase (tetragonal titanium dioxide).

TABLE 2

Surface Molar Composition of ZrO_2–TiO_2 (Zr/Ti = 1) Preparations Determined by EDX

Sulfate[a]/pretreatment[a] temp. (K)/crystallinity[b]	TiO_2	ZrO_2	SO_3	SO_3[c]
Nonsulfated/383 K/A	84.6	15.4	—	—
Nonsulfated/823 K/A	49.1	50.9	—	—
Nonsulfated/923K/C[d]	50.5	49.5	—	—
Sulfated/383 K/A	62.7	28.1	9.2	—
Sulfated/823 K/A	60.2	23.8	16.0	10.2
Sulfated/923 K/A	57.8	38.8	3.4	5.5
Sulfated/973 K/C[d]	65.5	31.8	2.7	1.7

Note. A, amorphous; C, crystalline.

[a] Hydroxide precipitate was dried at 383 K overnight. Sulfated samples were prepared by contacting dried samples with H_2SO_4, drying, and pretreating in air at elevated temperature for 3 h.

[b] Determined by X-ray diffractometry.

[c] Calculated from the TG curve, mol%.

[d] $TiZrO_4$.

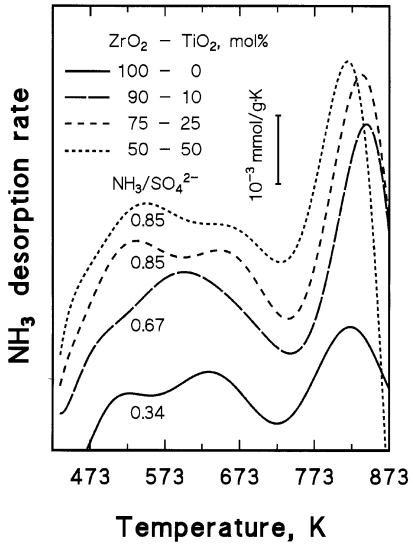

FIG. 3. Microbalance NH_3 TPD curves of sulfated ZrO_2 and ZrO_2–TiO_2 catalysts precalcided at 823 K. Sample was evacuated *in situ* in the balance at 773 K for 1 h, contacted with a flow of 2% NH_3/He mixture at 293 K for 1 h, and flushed then with pure He flow for 1 h. Temperature was ramped then at a rate of 10 K/min. The total amount of NH_3 desorbed was related to the sulfate content obtained by the separate thermogravimetric analysis of the catalyst.

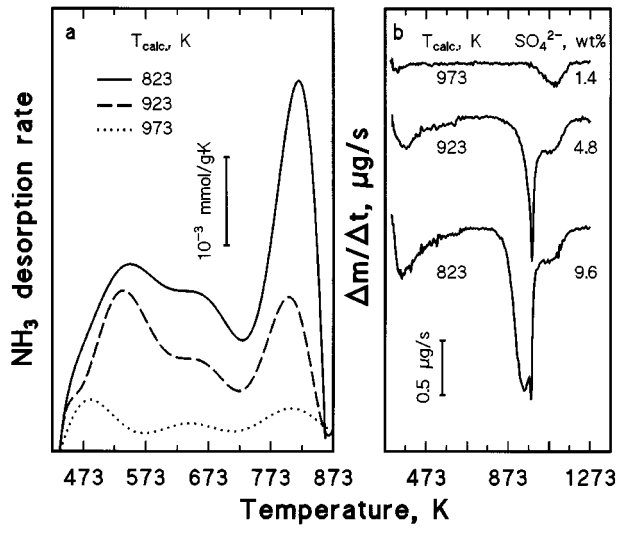

FIG. 4. NH_3 TPD (a) and DTG (b) curves of sulfated ZrO_2–TiO_2 (Zr/Ti = 1) catalysts precalcined in air at different temperatures ($T_{calc.}$) for 3 h. For details see legends to Figs. 1 and 3.

difference prevails between the composition of the bulk and the surface of the sulfated preparation even following high-temperature treatments.

Acidic Properties

Similar NH_3 TPD curves were obtained for all the sulfated zirconia and zirconia–titania samples (Fig. 3). Two temperature ranges assigned to ammonia bound to sites of medium and strong acidity were distinguished: the 420–720 K region with two or three broader peaks and the region above 720 K containing a narrower peak with a maximum at about 820–840 K, respectively. Although the sulfate content of the preparations is about the same, the integrated area of the desorption peaks, which is proportional to the amount of NH_3 desorbed, is different for the samples of different oxide composition. The TiO_2–ZrO_2 samples release more ammonia than the pure zirconia; furthermore, the presence of the second oxide seems to increase the relative intensity of the high-temperature desorption peak.

The acidic properties were modified by thermally decomposing the sulfate to different extents. The residual sulfate content of the samples was determined by thermogravimetric measurements (Fig. 4b). The NH_3 TPD curves obtained are shown in Fig. 4a. The amount of ammonia desorbed from surface sites of either medium or high acid strength changes parallel with the decreasing sulfate content and also the decreasing surface area, which, as it was shown in Table 1, occurs concomitantly with the sulfate loss.

In accordance with earlier studies a strong band was observed in the IR spectra of sulfated and dehydrated oxides at 1382 cm^{-1} (Fig. 5a). It was assigned to the high-frequency $\nu_{S=O}$ stretching band of surface sulfate groups of strongly covalent character. Adsorption of pyridine causes an approximate 75 cm^{-1} red shift of the band. On removing the

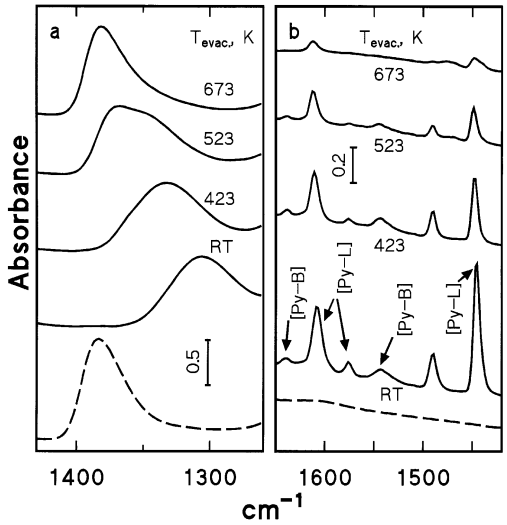

FIG. 5. The $\nu_{S=O}$ IR band of sulfated ZrO_2–TiO_2 (Zr/Ti = 1) catalyst before and after adsorption of pyridine (a) and the spectra obtained from the adsorbed pyridine (b). Self-supporting pellet was prepared from the sample precalcined at 823 K. It was treated in O_2 flow at 773 K in the IR cell for 1 h, evacuated, and contacted with 2 Torr pyridine at room temperature (RT) for 5 min. Spectra were recorded at RT after evacuation (dashed curves) and pyridine adsorption (RT) and after each subsequent 1-h evacuation at the temperature indicated. Absorbance is normalized to 10 mg/cm^2 thickness.

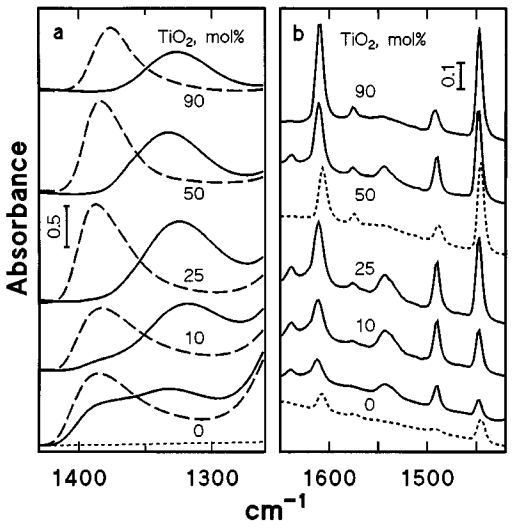

FIG. 6. The $\nu_{S=O}$ IR band of sulfated ZrO_2 and ZrO_2–TiO_2 catalysts before (dashed curves) and after (solid curves) adsorption of pyridine (a) and the spectra obtained from the adsorbed pyridine (b). The spectra of samples holding pyridine were recorded after evacuation at 423 K. The spectrum of nonsulfated ZrO_2 is given for reference (flat dashed line at the bottom of (a)). Spectra of pyridine adsorbed on sulfate-free mixed oxides are given for comparison (dashed curves in (b)). For conditions of pretreatment and adsorption see legend to Fig. 5.

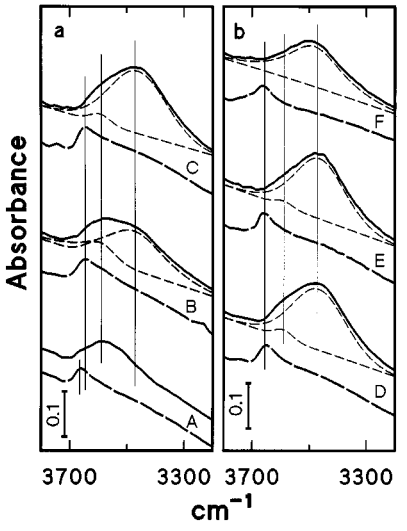

FIG. 7. The $\nu_{S=O}$ IR bands of nonsulfated ZrO_2 (A), sulfated ZrO_2 (B), and sulfated ZrO_2–TiO_2 containing 10 (C), 25 (D), 50 (E), and 90 (F) mol% TiO_2. Spectra were recorded in the absence (dashed curves) and in the presence (solid curves) of 5-Torr benzene vapor in the IR cell. For conditions of pretreatment see legend at Fig. 5. The thin dashed curves under the solid spectra represent the calculated component bands.

pyridine by evacuation at elevated temperatures the S=O band was found to shift gradually back to its original position (Fig. 5a).

Pyridine is forming different adsorption complexes with acid sites of Brønsted and Lewis type (e.g., 28). The spectra of pyridine adsorbed on sulfated ZrO_2–TiO_2 mixed oxide (Zr/Ti = 1) show clearly that both Lewis and Brønsted acidic sorption centers must be present in the sample (Fig. 5b).

Results of similar IR examinations are shown for different ZrO_2–TiO_2 compositions in Fig. 6. In absence of adsorbed pyridine, the position of the $\nu_{S=O}$ stretching band is about the same for each sample, viz, it appears at about 1380 cm^{-1} (Fig. 6a). The intensity of the band corresponds to the sulfate content; consequently, it is the smallest for the sample containing 90% TiO_2 (cf. Fig. 6a and Fig. 1a). On influence of the chemisorbed pyridine the band shifts to lower wavenumbers (Fig. 6a). Sulfated ZrO_2 seems to be an exception. In this case two smaller intensity sulfate peaks are generated. One of the peaks holds the position of the original sulfate band, indicating that all the sulfate may not have been accessible for pyridine in this sample. As it can be seen in Fig. 6b, both the Lewis and the Brønsted acidity increases with increasing titania content up to about 50 mol% TiO_2, but, the influence on the Lewis acidity is more pronounced.

The effect of adsorbed benzene on the ν_{OH} IR bands of nonsulfated and sulfated zirconia and also on sulfated ZrO_2–TiO_2 are shown in Fig. 7. Before adsorption of benzene no distinctly different surface OH bands can be distinguished (Fig. 7). *Note bene*, in the presence of sulfate the OH band was somewhat more intense than the corresponding band of the nonsulfated sample and it appeared at a frequency of about 25 cm^{-1} lower. Upon adsorption of benzene the band shifted substantially to lower wavenumbers. In accordance with earlier findings (e.g., 29), the integrated absorption coefficient increased and the band broadened. A red shift of about 70 cm^{-1} was observed for nonsulfated zirconia. The band obtained could not be resolved into component bands by computer program (Fig. 7a, spectra A). In contrast, the shifted broad band of sulfated zirconia could be resolved into two peaks (Fig. 7a, solid B and dashed curves under). The shifts of the components induced by adsorption of benzene are about 70 and 185 cm^{-1}. The position of the less-shifted band is about the same as that of the benzene-influenced OH groups of the nonsulfated sample (cf. Fig. 7a, solid A and B). The intensity of this component decreases with increasing TiO_2 content. In contrast, the more-shifted component band is stronger for the titania-containing mixed oxides than for the pure zirconia (Fig. 7).

Like pyridine the adsorbed benzene is also inducing a red shift of the $\nu_{S=O}$ stretching band (Fig. 8). The shift is about 15 cm^{-1}.

Catalytic Properties

The activity in the conversion of hexane is often used for characterizing catalyst acidity (e.g., 30). On samples of the present work two types of *n*-hexane transformations were

TABLE 3

Conversion of *n*-Hexane over Sulfated ZrO_2–TiO_2 Catalysts and H-Zeolites[a]

	823 K[b]				923 K[b]			
Catalyst	C[c] (mol%)	$r_a \times 10^{6}$[d] (mol h^{-1} m^{-2})	(c/i)[e]	(d/m)[f]	C[c] (mol%)	$r_a \times 10^{6}$[d] (mol h^{-1} m^{-2})	(c/i)[e]	(d/m)[f]
SO_4^{-2}/ZrO_2	5.3	0.110	0.70	0.24	3.8	0.064	1.15	0.25
SO_4^{-2}/90 mol% ZrO_2–TiO_2	13.9	0.163	1.17	0.25	5.4	0.068	1.21	0.26
SO_4^{-2}/75 mol% ZrO_2–TiO_2	19.2	0.150	1.62	0.27	2.5[g]	0.034	0.89	0.27
SO_4^{-2}/50 mol% ZrO_2–TiO_2	20.0	0.117	2.26	0.28	0.4[h] 0.0[i]	0.001	0.40	0.10
SO_4^{-2}/10 mol% ZrO_2–TiO_2	6.9	0.081	1.08	0.26	0.0	0.0	—	—
LZ-Y82[j]	0.4[k]	—	0	0.17	—	—	—	—
H-ZSM-5[l]	28.0[k]	—	5.2	0.04	—	—	—	—

Note. Reaction temperature, 423 K; WHSV $= 1.3 \times 10^{-2}$ g h^{-1} $g_{cat.}^{-1}$.

[a] Reaction products were analyzed after 5 min reaction time.

[b] Pretreatment temperature.

[c] Conversion.

[d] Areal rate of reaction calculated using the BET surface area given in Table 1.

[e] Cracking to isomerization molar ratio.

[f] The molar ratio of di- and monobranched hexane isomers.

[g] The highest conversion obtained after 20 min.

[h] The WHSV was decreased to 0.26×10^{-2} g h^{-1} g_{cat}^{-1} to get measurable conversion.

[i] Pretreated at 973 K.

[j] Dealuminated H–Y zeolite from Union Carbide Co., pretreated at 773 K, Si/Al = 5.2.

[k] Reaction products were analyzed after 30 min reaction time.

[l] Pretreated at 773 K; Si/Al = 15.5.

observed: cracking and isomerization. Ethane, propane, *n*- and *i*-butane, and *n*- and *i*-pentane were found and accounted as cracking products, while isomerization resulted in 2,2- and 2,3-dimethylbutane and 2- and 3-methylpentane. No unsaturated hydrocarbons were formed. Analysis for methane was not made. The results are given in Table 3.

On sulfated ZrO_2–TiO_2 catalysts pretreated at 823 K the conversion and also the cracking to isomerization ratio strongly increases with the TiO_2 content up to about 50 mol%. Due to loss of surface area and sulfate, catalysts pretreated at 923 K are much less active.

The activity of H-Y and H-ZSM-5 zeolites was also determined. The direct comparison of the results with those obtained for zirconia can be misleading since about 30–50% of the feed was retained by the zeolite in the first few minutes. After a 30-min time-on-flow zeolites became saturated and the activity determined was taken as catalytically meaningful (Table 3).

DISCUSSION

The addition of sulfate to zirconia was found to increase the thermal resistance of the high surface area amorphous or crystalline phases against sintering (e.g., 6). It was also shown that amorphous ZrO_2–TiO_2 mixed oxides get crystalline at higher temperature than pure ZrO_2 (27). In these respects the behavior of the catalysts used in the present study (Table 1) is in general agreement with that reported earlier, indicating that the effect of sulfate and titania on the thermochemical properties of the oxides is hardly dependent on minor variations in the preparation process of the sample.

Sulfated titania was shown to lose sulfate at a temperature of about 200 K lower than sulfated zirconia does (27). It seems possible, therefore, that sulfate is preferentially bound to zirconia and may shield this zirconia from being observed by EDX (Table 2). However, more has to be learned about the surface distribution of sulfate to substantiate this picture.

The specific surface area of sulfated zirconia–titania varies with the composition. A quite similar composition dependence of area was found for identically pretreated, but, nonsulfated samples (26). The close correspondence of the data suggests that the surface area of the sulfated mixed oxides is controlled rather by the titania than the sulfate.

The thermoanalytical curve of the X-ray amorphous sulfated zirconia (Fig. 1) shows that two kinds of sulfate species of different decomposition kinetics can be distinguished. For a crystalline preparation a similar result was obtained

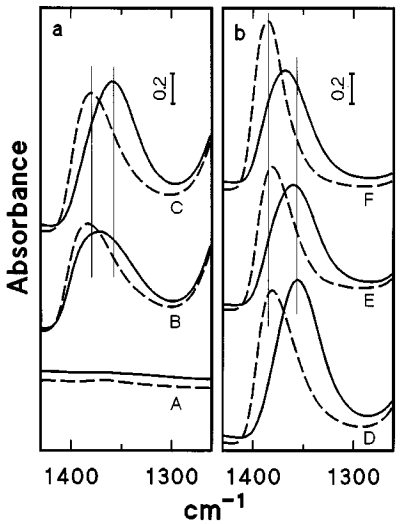

FIG. 8. The $\nu_{S=O}$ IR bands of nonsulfated ZrO_2(A), sulfated ZrO_2(B), and sulfated ZrO_2–TiO_2 containing 10 (C), 25 (D), 50 (E), and 90 (F) mol% TiO_2. Spectra were recorded in the absence (dashed curves) and in the presence (solid curves) of 5-Torr benzene vapor in the IR cell. The spectra were recorded in the same experiments as those shown in Fig. 7.

and interpreted by Morterra *et al.* (6), assuming that sulfate groups of different thermal stability are present in crystallographically regular and defective surface locations. Our data suggest that in our amorphous preparation the thermally more stable species is probably in the bulk while the less stable can be present in the surface layer. Latter is exposed to interaction with adsorbed pyridine. The adsorption of pyridine induces a shift in the infrared $\nu_{S=O}$ band, while the band of the sulfate present probably in the bulk appears unchanged (Fig. 6). For the titania-containing mixed oxides the intensity of the high-temperature decomposition peak is smaller than for zirconia (Fig. 1), furthermore, practically the whole sulfate band responds by shift on adsorption of pyridine, suggesting that in these higher-surface preparations most of the sulfate is in locations accessible for adsorption. Neither the original position nor the pyridine-effected shift of the $\nu_{S=O}$ band was modified by the presence of titania in the samples (Fig. 6).

The decomposition of the sulfate takes place simultaneously with the crystallization of the zirconia. In earlier works this phenomenon was not fully clarified [Ref. 5 and papers cited therein]. The sulfate decomposition and the effect of sulfate on the concomitant exothermic amorphous-to-crystalline transition of zirconia has been described, but, it was not considered that the net thermal effect is most probably the result of the two simultaneous processes. At the same sulfate level both the surface area and the rate of crystallization could be increased by increasing the amount of the titania component. This may explain that the sharp peak of crystallization and the broad sulfate decomposition peak can be distinguished on the DTA curves of the mixed oxides containing 25–50 mol% TiO_2 (Figs. 1a and 1b).

The NH_3 TPD curves of sulfated zirconia shown in Fig. 3 are similar to those found by Corma *et al.* (5). Comparing the data with those obtained for strongly acidic mordenite (31), it was suggested that the peak around 820 K might correspond to desorption of NH_3 from superacidic sites (5). In the zirconia–titania catalysts new type of acidic center was not revealed (Fig. 3), but, the 820 K peak attributed to the strongest acidic centers was found to grow more rapidly with the increasing titania content and the concomitantly increasing surface area than the other peaks. Also the number of sulfate species available for interaction with NH_3 increases, as it is shown by the NH_3/SO_4^{-2} ratios in Fig. 3.

The IR spectra of pyridine adsorbed on sulfate-free samples show the bands of Lewis bound pyridine only. These bands appear at wavenumbers of about 5 cm^{-1} lower than the corresponding bands obtained for the sulfated samples, indicating that stronger Lewis acid sites were induced by the presence of sulfate. Also Brønsted acid sites of acid strength able to protonate pyridine were invariably detected in all sulfated sample (Figs. 5b and 6b). The relative intensity of the bands attributed to pyridine bound to Lewis-acid sites changes parallel with the titania content. This correlation corresponds to that found for the 820 K TPD peak of NH_3, suggesting that the strongest acidic centers are of the Lewis type. This assignment is in agreement with that suggested earlier for the similar high-temperature NH_3 desorption peak of dealuminated mordenite (31). The lower-temperature TPD peaks of mordenite were shown to belong to desorption from strong Brønsted acidic sites. Considering cited results the same assignment can be substantiated for the peaks at about 600–640 K in Figs. 3 and 4a. The role of sulfate in generating the strongest acid sites is demonstrated by Fig. 4a. The sulfate content and the surface area were decreased by thermal treatment. The total acidity characterized by the amount of ammonia adsorbed decreased correspondingly; however, the decrease of the relative intensity of the peak assigned to the most strongly bound ammonia is obvious. This cannot be explained by the surface loss, but, by the decreasing amount of the sulfate groups which can be the strongly acidic sites or can generate such sites.

The chemisorption of the strong-base pyridine resulted in the perturbation of the sulfate species as indicated by the large red shift of the $\nu_{S=O}$ band (Fig. 6a). Jin *et al.* (14) considered this effect indirect. It was suggested that pyridine was bound to Lewis-acidic metal cations. These cations are thought to have Lewis acidity enhanced by the inductive effect of the sulfate groups. The chemisorbed pyridine can backdonate electrons through the metal cation to the sulfate group changing the character of the highly covalent S=O bond to more ionic. This change induces the shift of the $\nu_{S=O}$ band toward lower frequencies.

There is a general agreement that sulfated zirconia is a strong solid acid. Catalytic tests for acid catalyzed reactions, such as isomerization and cracking of alkanes or oligomerization of olefins suggest that the catalytic activity and presumably also the acidity of sulfated zirconia and strongly acidic zeolites and comparable (5, 21, 22). Test results for *n*-hexane conversion given in Table 3 are essentially in accordance with above conclusion. Nonsulfated catalysts are inactive. Sulfate is generating strong acidity, but, at the same sulfate content the presence of titania additive is increasing the weight-specific amount of acidic surface sites by stabilizing higher surface area. The variation of the areal reaction rate suggests that the number of active sites is not proportional to the surface area, but to the number of the active sulfate groups or rather to the number of the induced strong Brønsted acid sites accessible for the reactant. In the samples of smallest surface area (0–10 mol% TiO_2) not all the sulfate is accessible for ammonia and pyridine as it is demonstrated in Figs. 3 and 6. In these samples a fraction of the OH is weakly acidic and probably inactive in the reaction (Fig. 7a). In the samples of higher surface area (25–50 mol% TiO_2) most of the sulfate is located at accessible surface location; i.e., the amount of surface sulfate is practically equal with the total sulfate content. The amount of the sulfate-induced strongly acidic OH groups and the catalytic activity changes parallel with the amount of sulfate on the surface. As a result the weight specific rate of hexane conversion over the mixed oxides increases up to a titania content of about 25 mol%. Since the total sulfate content of the samples is about the same the areal sulfate and the strongly acidic OH concentration must be smaller for the higher surface area samples. This is reflected by the decreasing areal reaction rate (Table 3). The cracking of *n*-hexane demands strong acidic centers (30). The higher cracking to isomerization ratio obtained for catalysts containing more titania (up to 50 mol% Ti) suggest that the relative number of the strongest acidic centers is increasing preferentially if surface area increases. While the weight-specific activity changes with the composition of the catalyst, the molar ratio of the di- and monobranched hexanes (*d/m*) is practically independent of the titania and sulfate content. The invariable (*d/m*) ratio suggests that active sites of isomerization must be of similar acid strength in the different catalysts. As it could be expected the formation of the dibranched isomers is not favored within the narrow pores of zeolites.

The views about the acid strength of zirconia are most contradictory. The methods using basic probes, applied successfully for defining the acid strength of zeolites on a relative scale, usually provided with inconsistent results when comparison of acidity for zirconia and zeolites was attempted (5, 21).

In interaction with acidic surface OH groups the strong base pyridine can be protonated while the corresponding OH bands disappear from the IR spectra. Therefore, pyridine is good probe for detecting the existence of Brønsted acidic sites, but, based on the IR spectra only, not much can be learned about the acid strength of the sites (Figs. 5 and 6). The weaker base benzene can link to the same OH groups by hydrogen bonds. By its adsorption a red shift of the OH band is induced which can be used as a convenient measure of the strength of the interaction and, thereby, can be used as a parameter correlating with the acid strength of the Brønsted centers (29). In fact, other probe molecule methods developed on the basis of H^1 MAS NMR or UV spectroscopic measurements employ similar approach to the problem (21, 39).The adsorption of weak-base probe which is not protonated under the experimental conditions is applied to induce the shift of the proton NMR signal or the red shift of a UV band of the appropriate adsorbate. These shifts are used again for characterizing the acid strength.

On adsorption of benzene the IR band of the OH groups of zirconia shifted with about 70 cm^{-1} to lower wavenumbers (Fig. 7a, spectra A). The 185 cm^{-1} shift found for the sulfated catalyst suggests that sulfate generated new acidic OH groups of considerably stronger acidity. In agreement with the NH_3 TPD results discussed above the addition of titania as a second oxide did not generate new acidic centers, but, as indicated by the higher intensity of the more shifted component band, the concentration of the stronger Brønsted acidic center was increased (Fig. 7). The corresponding shift for dealuminated zeolite H-Y or H-ZSM-5 was larger by about 100 cm^{-1} than that obtained for sulfated zirconia. Would it mean that zeolites are much stronger acids? In this case how can catalytic activity measurements be interpreted?

It is well known that the strength of a Brønsted acid is enhanced if the size of its conjugate base wherein the negative charge can be delocalized is increased. In acidic zeolites, for instance, the stability and also the surface concentration of a protonated base, which is a measure of the acid strength, depend on the volume of the zeolite lattice relative to the number of the Brønsted sites. The negative charge on the lattice is increased each time when an essentially covalently bound hydrogen is donated as a proton and, as a consequence, the acidity of the remaining sites is reduced (32, 33). In order to measure the unperturbed strength of the strongest sites generally a minute amount of the weakest base Hammett indicator that still can be protonated by the catalyst is added to a large excess of acid sites (33). Another approach, as mentioned above, it is use of weakly basic probe, which is not protonated by the solid, and correlating the acidity with the strength of the adsorbate–acid site interaction (32).

Both the Brønsted- and the Lewis-bound pyridine increase the negative charge on the conjugated base of the Brønsted acid sulfated zirconia. The electrons are delocalized to some extent on the sulfate groups as it is indicated

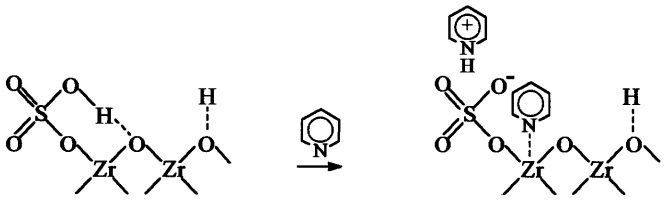

SCHEME 1

by large red shift of the $\nu_{S=O}$ IR band (Fig. 6). Scheme 1 is proposed for describing the possible chemistry.

The HSO_4^- anion, carrying a hydrogen atom linked through a hydrogen bond to the oxygen of the zirconia support, is a strong Brønsted acidic site, whereas the surface OH group of the zirconia support represents weaker acidic site. The existence of these two kinds of sites could be substantiated by IR spectroscopy following benzene adsorption (Fig. 7).

A similar, but smaller red shift of the $\nu_{S=O}$ band was observed upon adsorbing the less basic benzene, indicating that in these cases electrons were also donated by the probe molecule. In absence of protonation the negative charge can be increased on the sulfate mainly by electron transfer from the zirconium cations carrying adsorbed benzene (Fig. 8). In other words, the basicity of the conjugate base of the proton is increased, resulting in a weaker interaction between the Brønsted acidic site and benzene molecule. The acid strength of the Brønsted acidic center is probably smaller against benzene than it is against the even weaker base alkanes.

The shift of the $\nu_{S=O}$ IR band was shown to be useful for indicating any change in the negative charge concentration on the conjugated base of the sulfated-oxide solid acids. The electron density of the zeolitic lattice may also change even on adsorption of a weak base like benzene; however, for this we do not have direct experimental evidence. The comparable activities of the catalysts in the conversion of alkanes may suggest that these systems are of comparable acidity. In this case the larger red shift of the zeolite OH band on adsorption of benzene may indicate only that benzene donated less electrons to the lattice and/or the electrons were delocalized in a larger volume.

CONCLUSION

The nonsulfated zirconia contains only weak Brønsted acidic sites, while new stronger Brønsted acidic sites are also present in the sulfated samples. The addition of titania as a second oxide to zirconia hinders the aggregation of the oxide components. It modifies the extensive, but not the intensive, acidic properties of the sulfated catalysts. With the increasing surface area the amount of both the sulfate and the strong acid centers accessible for adsorption increases. The strongest acidic sites are centers of Lewis-acid type.

The adsorption of a base regardless of whether it is protonated or not increases the negative charge on the conjugated base of the solid Brønsted acid. For zeolites this process may remain unobserved; however, it is clearly shown by the red shift of the $\nu_{S=O}$ IR band of the sulfated oxides. As a result the adsorption decreases the acid strength of the proton and also the strength of the proton–base interaction. The extent of this effect depends on the degree of electron donation and on the volume available for the delocalization of the negative charge. Results suggest that parameters characteristic for the strength of acid–base interaction and, thereby, also for the acid strength should be handled cautiously when they are used for comparing the acidity of catalyst systems much different in structure and composition, such as zeolites and sulfated zirconia.

ACKNOWLEDGMENTS

One of the authors (F.L.) expresses his appreciation for the fellowship provided by the Agency of Industrial Science and Technology, Ministry of International Trade and Industry, Japan. Thanks is due to Mr. Yoshimichi Kiyozumi (NIMCR, Tsukuba, Japan) for his assistance in obtaining the EDX spectra and to J. Varga (CRIC, Budapest, Hungary) for providing us with his computer program for resolving IR bands.

REFERENCES

1. Olah, G. A., Surya Prakash, G. K., and Sommer, J., "Superacids," Wiley, New York, 1985.
2. (a) Tanabe, K., *in* "Catalysis: Science and Technology," Vol. 2. p. 231. Akademie-Verlag, Berlin, 1983; (b) Tanabe, K., Misono, M., Ono, Y., and Hattori, H., "New Solid Acids and Bases," Kodansha-Elsevier, Tokyo, 1989.
3. (a) Hino, M., and Arata, K., *J. Chem. Soc. Chem. Commun.* 1148 (1979); (b) Ibid, 851 (1980); (c) Hino, M., and Arata, K., *Chem. Lett.* 1259 (1979).
4. (a) Yamaguchi, T., *Appl. Catal.* **61**, 1 (1990); (b) Scurrell, M. S., *Appl. Catal.* **34**, 109 (1987).
5. Corma, A., Fornés, V., Juan-Rajadell, M. I., and López Nieto, J. M., *Appl. Catal.* **116**, 151 (1994).
6. Morterra, C., Cerrato, G., Emanuel, C., and Bolis, V., *J. Catal.* **142**, 349 (1993).
7. Nascimento, P., Akratopoulou, C., Oszagyan, H., Coudurier, G., Travers, G., Joly, J.-F., and Vedrine, J. C., *Stud. Surf. Sci. Catal.* **75**, 1185 (1993).
8. Chen, F. R., Coudurier, G., Joly, J.-F., and Vedrine, J. C., *J. Catal.* **143**, 616 (1993).
9. Comelli, R. A., Vera, C. R., and Parera, J. M., *J. Catal.* **151**, 96 (1995).
10. Sohn, J. R., and Kim, H. W., *J. Mol. Catal.* **52**, 361 (1989).
11. Parera, J. M., *Catal. Today* **15**, 481 (1992).
12. Ward, D. A., and Ko, E. I., *J. Catal.* **150**, 18 (1994).
13. Tanabe, K., *in* "Heterogeneous Catalysis" (Shapiro, B. L., Ed.), p. 71. Texas A&M Univ. Press, College Station, TX, 1984.
14. Jin, T., Yamaguchi, T., and Tanabe, K., *J. Phys. Chem.* **90**, 4794 (1986).
15. Bensitel, M., Saur, O., Lavalley, J.-C., and Morrow, B. A., *Mater. Chem. Phys.* **19**, 147 (1988).
16. Waqif, M., Bachelier, J., Saur, O., and Lavalley, J.-C., *J. Mol. Catal.* **72**, 127 (1992).
17. Bolis, V., Morterra, C., Volante, M., Orio, L., and Fubini, B., *Langmuir* **6**, 695 (1990).

18. Morterra, C., Orio, L., Bolis, V., and Ugliengo, P., *Mater. Chem. Phys.* **29**, 457 (1991).
19. Sun, Y., Chu, P.-J., and Lunsford, J. H., *Langmuir* **7**, 3027 (1991).
20. Riemer, T., Spielbauer, D., Hunger, M., Mekhemer, G. A. H., and Knözinger, H., *J. Chem. Soc. Chem. Commun.* 1181 (1994).
21. Adeeva, V., de Haan, J. W., Jänchen, J., Lei, G. D., Schünemann, V., van de Ven, L. J. M., Sachtler, W. M. H., and van Santen, R. A., *J. Catal.* **151**, 364 (1995).
22. Kustov, L. M., Kazansky, V. B., Figueras, F., and Tichit, D., *J. Catal.* **150**, 143 (1994).
23. (a) Hsu, C.-Y., Heimbuck, C. R., Armes, C. T., and Gates, B. C., *J. Chem. Soc. Chem. Commun.* 1645 (1992); (b) Lin, C.-H., and Hsu, C.-Y., *J. Chem. Soc. Chem. Commun.* 1479 (1992).
24. Adeeva, V., Lei, G. D., and Sachtler, W. M. H., *Appl. Catal.* **118**, L11–L15 (1994).
25. Mercera, P. D. L., van Ommen, J. G., Doesburg, E. B. M., Burggraaf, A. J., and Ross, J. R. H., *Appl. Catal.* **471**, 363 (1991).
26. (a) Wang, I., Chang, W.-F., Shiau, R.-J., Wu, J.-C., and Chung, C.-S., *J. Catal.* **83**, 428 (1983); (b) Lahousse, C., Aboulayt, A., Maugé, F., Bachelier, J., and Lavalley, J. C., *J. Mol. Catal.* **84**, 283 (1993).
27. Lónyi, F., and Valyon, J., *J. Therm. Anal.* **46**, 211 (1996).
28. Parry, E. P., *J. Catal.* **2**, 371 (1963).
29. Datka, J., *J. Chem. Soc. Faraday Trans. 1* **77**, 511 (1981).
30. Sohn, J. R., DeCanio, S. J., Fritz, P. O., and Lunsford, J. H., *J. Phys. Chem.* **90**, 4847 (1986).
31. Karge, H. G., and Dondur, V., *J. Phys. Chem.* **94**, 765 (1990).
32. Umansky, B. S., Engelhardt, J., and Hall, W. K., *J. Catal.* **127**, 128 (1991).
33. Umansky, B. S., and Hall, W. K., *J. Catal.* **124**, 97 (1990).